



Design, synthesis, and biological evaluation of novel 6-(pyridin-3-yl)quinazolin-4(3H)-one derivatives as potential anticancer agents via PI3K inhibition

Huarong Yang^{a,b,1}, Qing Li^{a,c,1}, Mingzhi Su^{a,c}, Fang Luo^{a,c}, Yahua Liu^{b,**}, Daoping Wang^{a,c,**}, Yanhua Fan^{a,c,*}

^a State Key Laboratory for Functions and Applications of Medicinal Plants, Guizhou Medical University, Guiyang 550014, PR China

^b School of Pharmacy, Guizhou University of Traditional Chinese Medicine, Guiyang 550002, PR China

^c The Key Laboratory of Chemistry for Natural Products of Guizhou Province and Chinese Academy of Sciences, Guiyang 550014, PR China

ARTICLE INFO

Keywords:

6-(pyridin-3-yl)quinazolin-4(3H)-one derivatives
PI3K/Akt pathway
G2/M phase arrests
Cell apoptosis

ABSTRACT

Abnormal activation of the PI3K/Akt pathway is demonstrated in most of human malignant tumors via regulation of proliferation, cell cycle, and apoptosis. Therefore, drug discovery and development of targeting the PI3K/Akt pathway has attracted great interest of researchers in the development of anticancer drugs. In this study, fifteen 6-(pyridin-3-yl)quinazolin-4(3H)-one derivatives were designed and synthesized. Anticancer activities of the synthetic compounds were evaluated and the potential mechanisms were explored. Several compounds showed certain proliferation inhibitory activity against the tested cancer cells including human non-small cell lung cancer (NSCLC) HCC827, human neuroblastoma SH-SY5Y and hepatocellular carcinoma LM3 cells. Among them, compound **7i** and **7m** showed the best inhibitory activity against all the cancer cell lines and more active against HCC827 cells with IC₅₀ values of 1.12 μM and 1.20 μM, respectively. In addition, **7i** and **7m** showed lower inhibitory activity against H7702 cells (human normal liver cells) with IC₅₀ values of 8.66 μM and 10.89 μM, respectively, nearly 8-fold lower than that in HCC827 cells. These results suggested that compounds **7i** and **7m** had certain selectivity to tumor cells, compared to human normal cells. Further biological studies indicated **7i** induced G2/M phase arrests and cell apoptosis of HCC827 cells via PI3K/Akt and caspase dependent pathway. Together, these novel 6-(pyridin-3-yl)quinazolin-4(3H)-one derivatives such as compound **7i** and **7m** might be lead compounds for development of potential anti-cancer drugs.

1. Introduction

Quinazolin-4(3H)-one is a promising pharmacophore with versatile bioactivities for drug design and development, which is widely discovered in natural products.^{1,2} Researchers have developed numerous novel drugs on the market or candidates in the clinical trials based on Quinazolin-4(3H)-one moiety.^{3–5} Halofuginone is a quinazolinone alkaloid with potential anticancer activity due to its combined suppression of invasiveness, vascularization, and cell proliferation via multi-molecular mechanism including the mediation of PI3K/Akt.^{5–7} In addition to Halofuginone, there are many small-molecule inhibitors in preclinical or

clinical trials for cancer therapy including PI3K inhibitors such as Acalisib,⁸ Idelalisib⁹ and Tentalisib.¹⁰ For this purpose, Quinazolin-4(3H)-one derivatives are promising and useful PI3K inhibitors based on these previous studies.

PI3K can be divided into three categories, among them, class I PI3K have been extensively studied as one of the critical transducer signals of receptor tyrosine kinases (RTKs).^{11–14} Abnormal activation of PI3K/Akt pathway is identified in most of the human tumors via regulation of cell cycle, proliferation, and apoptosis.^{11–12} Mutations in members of the PI3K/Akt pathway commonly occurred in the *PIK3CA*, which encoded p110α catalytic subunit of PI3K.^{11–12,14–17} Tumors harboring *PIK3CA*

* Corresponding author at: State Key Laboratory for Functions and Applications of Medicinal Plants, Guizhou Medical University, Guiyang 550014, PR China.

** Corresponding author at: State Key Laboratory for Functions and Applications of Medicinal Plants, Guizhou Medical University, Guiyang 550014, PR China (D. Wang).

E-mail addresses: liuyahu145@gzy.edu.cn (Y. Liu), wangdaoping@gzcnpcn (D. Wang), yhfana@gzcnpcn (Y. Fan).

¹ These authors contributed equally to this work.

mutations correspondingly remain active upon upstream targets inhibition.^{14–17} In view of the key role of PI3K in tumorigenesis, development, and drug resistance of RTK inhibitors, inhibitors targeting PI3K signaling showed considerable anti-cancer activity and have achieved great success in cancer therapy in clinical studies.^{18–20}

Our research group has long been engaged in the development of anti-cancer drugs. In our previous study, we designed and synthesized a series of quinazolinone derivatives and obtained several lead compounds targeting PI3K and Aurora kinase.^{21–25} Quinazolinone has been identified as a promising scaffold for the development of kinase inhibitors, especially PI3K inhibitors.^{8–10,26–28} To discover more potential anti-cancer quinazolinone derivatives, we performed further structure optimization based on our previous findings and other known quinazolinone PI3K inhibitors via conjugate some of the related pharmacophore (Fig. 1). We also performed anticancer activity evaluation to identify the most active compound and most sensitive cell lines for the further investigation of possible mechanisms of action. As Fig. 1 described, PI3K inhibitors with Quinazolinone scaffold including PI3K α inhibitor DFX24 (IC₅₀ is 6.5 nM against PI3K α) and PI3K δ inhibitor Acalisib (IC₅₀ is 14 nM against PI3K δ),^{23,24,29} and expected our target compounds to maintain both PI3K α and PI3K δ kinase inhibitory activity. In addition, the inhibitor of mTOR XL388³⁰ was selected as the lead compound and attempted to strengthen the suppression of mTOR.

2. Results and discussion

2.1. Chemistry

The substituted quinazolin-4(3H)-one intermediates was synthesized from 2-amino-5-bromobenzoic acid. As shown in Scheme 1, two general methods A and B were used to synthesize the substituted quinazolin-4(3H)-one moiety. The alkylation of quinazolin-4(3H)-ones has been reported to afforded N³-substituted products or a mixture of N³- and O⁴-substituted products.³¹ However, only N³-substituted quinazolin-4(3H)-

ones was obtained in this study according to the reported conditions. As shown in Scheme 2, critical intermediates 6 was prepared via a Suzuki-Miyaura Cross-Coupling reaction. 6-bromoquinazolin-4(3H)-ones was treated with 5-(4,4,5,5-tetramethyl-1,3,2-dioxaborolan-2-yl) pyridin-2-amine to afford intermediates 6, and Pd(dppf)Cl₂ was chosen as a highly efficient catalyst. To our surprise, the cross-coupling reactions afforded the crucial intermediates 6 in good yields (above 80%). Finally, treatment of intermediates 6 with various acyl chlorides provided 3,6-disubstituted quinazolin-4(3H)-ones 7. Various substituents were introduced at the N³- and C⁶- positions of the quinazolin-4(3H)-one scaffold. Various amide derivatives were also synthesized to further explore the structure–activity relationship. All compounds were shown in Table 1.

2.2. Biological evaluation

2.2.1. Antiproliferation activity assay

In order to investigate the anti-proliferation activity of the synthetic compounds in cancer cell lines, cell viabilities of human non-small cell lung cancer (NSCLC) HCC827, human red and white cell leukemia cell HEL, human neuroblastoma SH-SY5Y and hepatocellular carcinoma LM3 cells treated with the synthetic compounds at various concentrations were measured by cell counting. As shown in Table 1 and Figs. S1–S2, the 15 evaluated compounds showed diverse anti-proliferation activity. Among them, compounds 7m and 7i significantly attenuated the cell growth of all the tested cancer cells with IC₅₀ values of 1.12 μ M and 1.20 μ M against HCC827 cells, respectively. We also evaluated the cytotoxicity of the most potent compound 7i and 7m on human normal liver HL-7702 cells to investigate their selectivity to tumor cell lines. As shown in Table 1 and Fig. S1–S2, both compound 7i and 7m showed lower inhibitory activities against HL-7702 cells (human normal liver cells) with an IC₅₀ values of 8.66 μ M and 10.89 μ M, which was nearly 8-fold lower than that in HCC827 cells. These results suggested that 7i and 7m had certain selectivity to tumor cells, compared to human normal

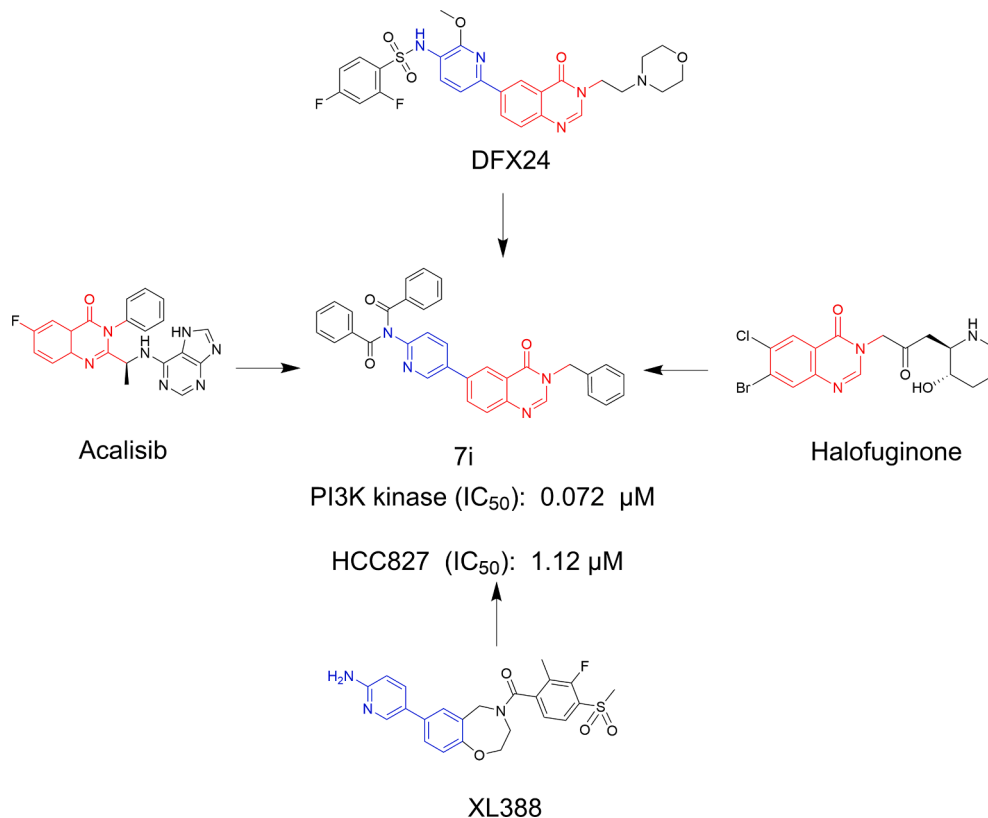
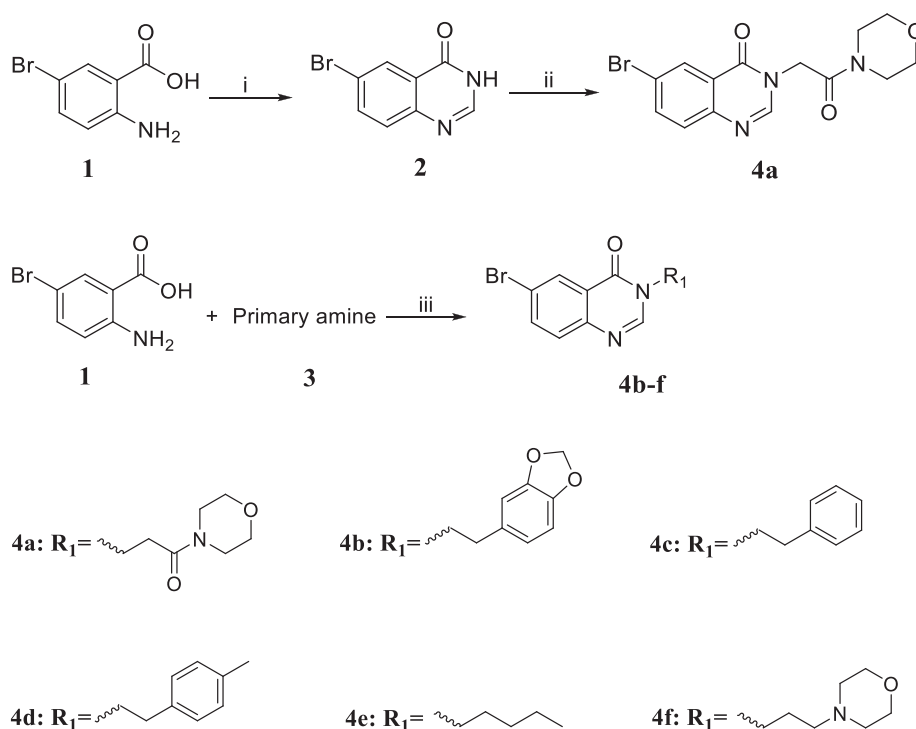
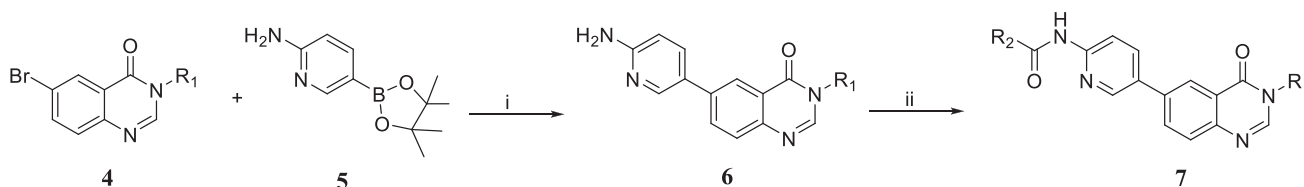


Figure 1. Diagram represents compounds design by molecular hybridization.



Scheme 1. (i) formamide, 130 °C, 4 h; (ii) alkyl halides, NaH, DMF, ambient temperature, overnight; (iii) triethyl orthoformate, I₂, EtOH, reflux, 6 h.



Scheme 2. (i) Pd(dppf)Cl₂, K₂CO₃, Dioxane/H₂O, 100 °C, 20 h; (ii) Acyl chloride, Et₃N, THF, 0 °C to ambient temperature, overnight.

cells. Since compound **7i** showed the best inhibitory activity against all the tested cancer cells, hence it was selected for the further mechanism study.

2.2.2. Effects of **7i** on PI3K/Akt pathway

Hyperactivation or mutation of the PI3K/Akt pathway has been demonstrated as a characteristic feature of various cancers including human non-small cell lung cancer (NSCLC),¹⁷ human neuroblastoma and hepatocellular carcinoma, which have led to the clinical development of PI3K kinase inhibitors for cancer therapy.^{32,33} In view of the lead compounds with quinazolinone scaffold of **7i** such as DFX24 and Acalisib showed PI3K inhibitory activity,^{25–28,31} we analyzed the protein alterations of the critical components of PI3K/Akt pathway including p-Akt, p-GSK3β and p-mTOR using western blot to explore the effects of **7i** at various dose on PI3K/Akt pathway. As shown in Fig. 2, phosphorylated levels of downstream targets including Akt, GSK3β and mTOR were completely suppressed, indicating the inhibition of PI3K/Akt pathway by compound **7i**.

To confirm whether the effect of **7i** on PI3K/Akt pathway was related to the PI3K kinase activity, PI3K kinase assay was performed PI3K phosphorylation evaluation in HCC827 cells using a cell PI3K assay kit. As shown in Table 2, **7i** markedly inhibited the total PI3K kinase activities with an IC₅₀ values of 0.072 μM. All these results showed **7i** might be a PI3K pathway inhibitor, at least in part due to its PI3K kinase inhibitory activity.

2.2.3. Molecular docking

To explore the potential binding mode of **7i** and the catalytic subunit of PI3K including PI3Kα (PDB entry code: 4ZOP) binding with its complex ligand (PDB ID: 4Q2), PI3Kβ (PDB entry code: 4BFR) binding with its complex ligand (PDB ID: J82), PI3Kγ (PDB entry code: 4ANW) binding with its complex ligand (PDB ID: O92) and PI3Kδ (PDB entry code: 4GB9) binding with its complex ligand (PDB ID: OWR), we performed molecular modeling studies. As depicted in Fig. 3 and Table S1, compound **7i** formed three hydrogen bonds with the critical residue Lys802 in catalytic sites, Gln859 in the side chain and Arg770 residues in the affinity pocket of PI3Kα, consistent with other PI3Kα inhibitors.^{34–36} Also, **7i** formed hydrophobic interactions with residues in side chains of PI3Kα. All these hydrogen bonds and hydrophobic interactions would stabilize the conformations and interactions between **7i** and PI3Kα. In addition, the potential binding mode of **7i** and PI3Kβ was also predicted by molecular docking study (Fig. 4). It was reported that the hydrogen bonds with the nitrogen of Val848 in the hinge region and the hydrophobic interactions with residues Ile797 and Ile930 in the hydrophobic region of ATP binding site was critical for the kinase inhibitory activity of PI3Kβ inhibitors.^{37,38} Importantly, the previous mutagenesis study showed that Try772 in the P-loop has played a pivotal role in selectivity for PI3Kβ. As shown in Fig. 4 and Table S1, **7i** formed hydrogen bonds or hydrophobic interactions with residues mentioned above and other different residues including Arg729, Lys771, Trp781 and Tyr833. Although, there are various interactions were formed between **7i** and PI3Kβ, they bind in a very different manner to what has been reported

Table 1
Cytotoxic activity (IC₅₀^a, μM) against cancer cell lines.

Comp.	Structure	HCC827	LM3	SH-SY5Y	HEL	HL-7702
7a		>40	>40	>40	>40	NT
7b		>40	>40	>40	>40	NT
7c		>40	>40	>40	>40	NT
7d		>40	>40	>40	>40	NT
7e		>40	>40	>40	>40	NT
7f		>40	>40	>40	>40	NT
7g		>40	>40	>40	>40	NT
7h		>40	>40	>40	>40	NT
7i		1.12 ± 0.11	2.65 ± 0.23	2.13 ± 0.19	2.01 ± 0.19	8.66 ± 0.61
7j		32.17 ± 0.15	>40	35.38 ± 0.22	18.84 ± 0.11	NT
7k		>40	>40	>40	>40	NT
7l		29.23 ± 0.13	>40	>40	>40	NT
7m		1.20 ± 0.17	2.49 ± 0.19	3.72 ± 0.21	2.83 ± 0.36	10.89 ± 0.57
7n		>40	>40	>40	>40	NT
7o		28.96 ± 1.91	>40	>40	>40	NT
BEZ235		0.53 ± 0.11	1.31 ± 0.25	0.79 ± 0.17	0.29 ± 0.09	NT

^a Data are expressed as mean ± SD from three different experiments. NT: Not tested.

for PI3Kβ specific inhibitors.^{37,38} Given the molecular docking score of **7i** (Scores = -7.94) is very close to that of its complex ligand J82 (Table S1), we guessed that the PI3Kβ kinase inhibitory activity of **7i** also contributed to its PI3K kinase inhibition. We further performed molecular modeling study to investigate the potential binding capability of **7i** and PI3Kγ. Unfortunately, docking of **7i** into the PI3Kγ binding pocket PI3Kγ showed that the pocket does not cover the structure of **7i** and showed much lower docking score with -6.04 compared to that of its complex ligand (Scores = -7.91), suggesting the less activity of **7i** against PI3Kγ (Fig. 5 and Table S1). Finally, we investigated the combining

capacity of **7i** and PI3Kδ. As shown in Fig. 6, the nondifferentiated binding mode of compound **7i** and OWR suggesting their similar PI3Kδ kinase inhibitory activity. In general, the data of molecular modeling study implied compound **7i** might showed PI3K kinase inhibitory activity mainly due to the inhibition of PI3Kα, PI3Kβ and PI3Kδ.

2.2.4. Effects of **7i** on cell cycle distribution

Mutation or abnormal levels of cell cycle related proteins and genes usually led to uncontrolled tumor cell cycle and sustained proliferation of tumor cells. There are also growing evidences that the PI3K pathway

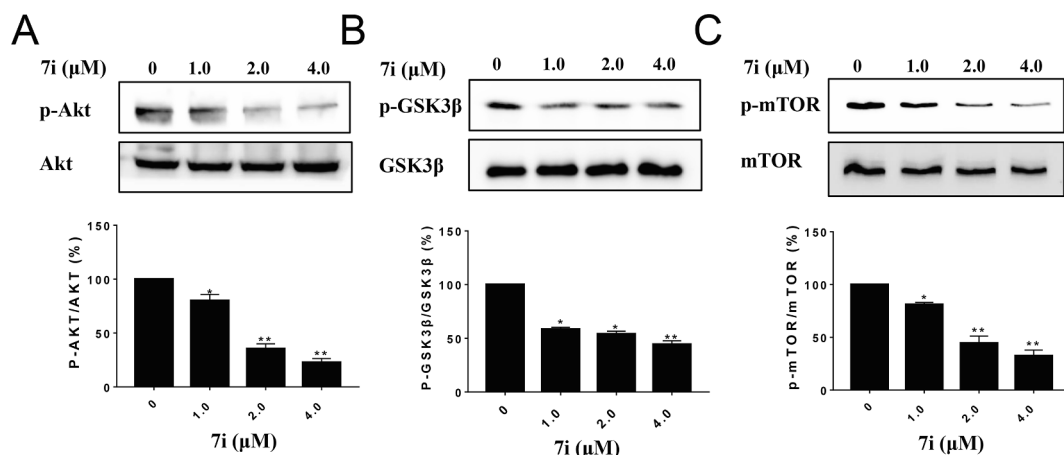


Figure 2. Compound **7i** inhibited PI3K signaling pathway. (A) **7i** decreased the phosphorylation levels of Akt at Ser473. (B) **7i** decreased the phosphorylation levels of GSK3 β at Ser9. (C) **7i** decreased the phosphorylation levels of mTOR at Ser2448. HCC827 cells were treated with different concentrations of **7i** for 24 h to evaluate the alteration of representative protein expression of PI3K pathway including p-Akt, p-GSK β and p-mTOR. Data are expressed as mean \pm SD from three parallel experiments (* p < 0.05, ** p < 0.01 vs DMSO control).

Table 2

Cell PI3 Kinase activity of compound **7i** (IC₅₀, μ M).

Name	PI3K inhibitory activity
7i	0.072 \pm 0.012
Wortmannin	0.018 \pm 0.006

IC₅₀ values are the mean \pm SD of three separate experiments.

Wortmannin is a known pan PI3K inhibitor.

plays a critical role in the regulation of the cell cycle. PI3K α inhibitor HS-173 has been found to induced G2 phase arrest. Therefore, we examined the effects of **7i** on cell cycle distribution. Consistent with our prior studies, **7i** also induced G2 cell cycle arrest in a concentration-dependent manner, and G1 phase was relatively decreased compared to that of the control groups (Fig. 7A-B). To further elucidate whether cell cycle arrest was related to the regulation of cell cycle checkpoint proteins, the expression of G2 cell cycle regulatory proteins was

determined by western blot analysis. Reduced expressions levels of CHK1, p-CHK1, c-Myc and Cyclin B1 were observed after **7i** treatment (Fig. 7B-7D).

2.2.5. Effects of **7i** on cell apoptosis

We next assessed the efficacy of **7i** on cell apoptosis in HCC827 cells. The presence of **7i** resulted in increased induction of cell apoptosis compared to that achieved by control group or lower dose treatments (Fig. 8A-B). To further clarify the molecular mechanisms of **7i** involved apoptosis, the effect of **7i** on the expression levels of apoptosis-associated proteins was examined by western blot analysis. In comparison to the vehicle-treated control group, the pro-apoptotic proteins cleaved-PRAP (Fig. 8C), cleaved-caspase 9 (Fig. 8D) and Bax (Fig. 8E) were upregulated by **7i** treatment in a concentration-dependent manner, but the anti-apoptotic protein Bcl-2 was downregulated (Fig. 8F). Taken together, these data suggested that **7i** induced apoptotic cell death via the mitochondrial (intrinsic) pathway in HCC827 cells.

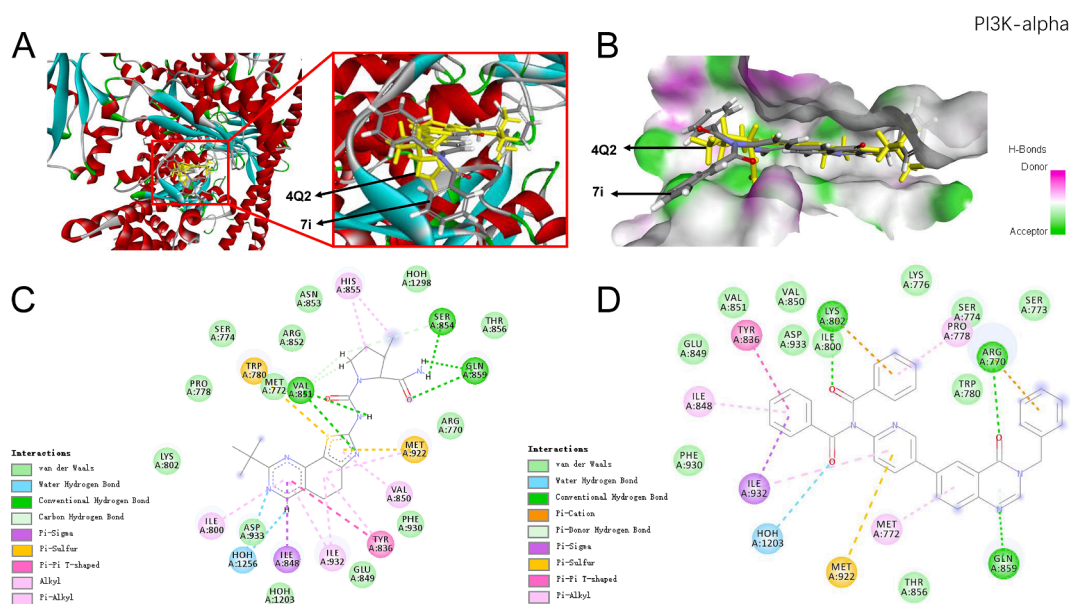


Figure 3. Docking model of compound **7i** in the PI3K α (PDB entry code: 4ZOP, the complex ligand 4Q2). (A) The bound conformations of compound **7i** and 4Q2 of PI3K α in the active site. (B) Compound **7i** and 4Q2 docked into the active pocket. (C) 2D binding model of 4Q2 and PI3K α . (D) 2D binding model of **7i** and PI3K α . The figure was generated using Accelrys Discovery Studio Visualizer 4.5.

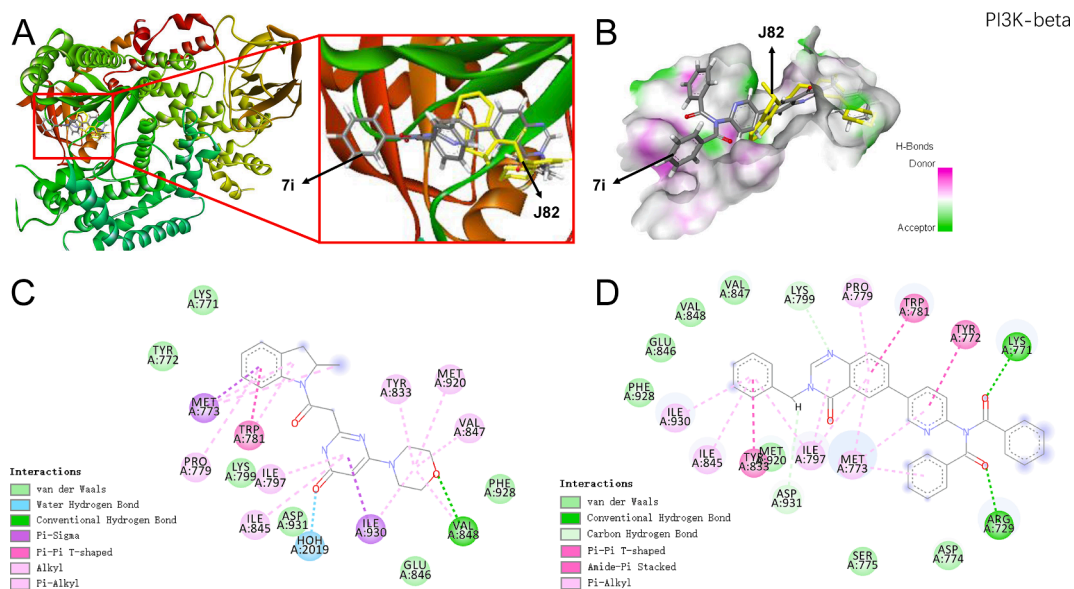


Figure 4. Docking model of compound **7i** in the PI3K β (PDB entry code: 4BFR, the complex ligand J82). (A) The bound conformations of compound **7i** and J82 of PI3K β in the active site. (B) Compound **7i** and J82 docked into the active pocket. (C) 2D binding model of **7i** and PI3K β . (D) 2D binding model of J82 and PI3K β . The figure was generated using Accelrys Discovery Studio Visualizer 4.5.

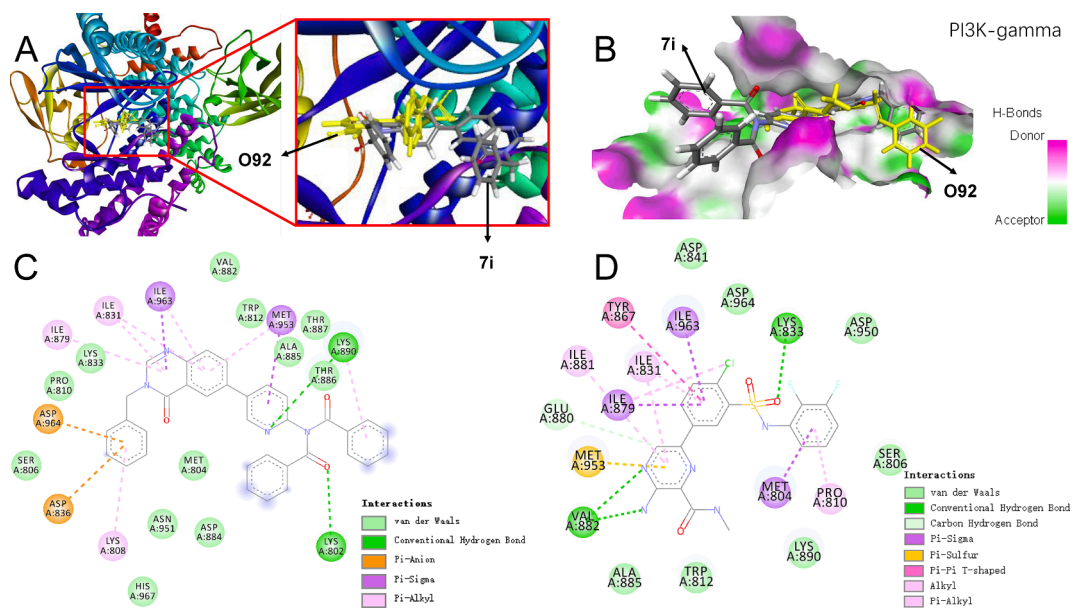


Figure 5. Docking model of compound **7i** in the PI3K γ (PDB entry code: 4ANW, the complex ligand O92). (A) The bound conformations of compound **7i** and O92 of PI3K γ in the active site. (B) Compound **7i** and O92 docked into the active pocket. (C) 2D binding model of **7i** and PI3K γ . (D) 2D binding model of O92 and PI3K γ . The figure was generated using Accelrys Discovery Studio Visualizer 4.5.

3. Materials and methods

3.1. Chemistry

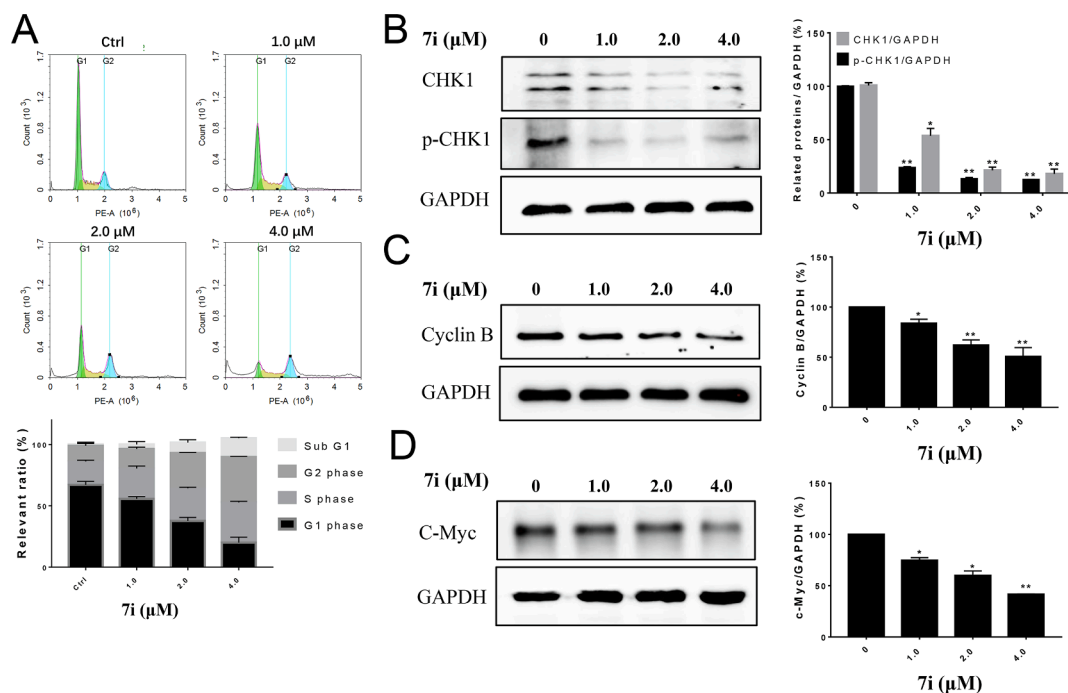
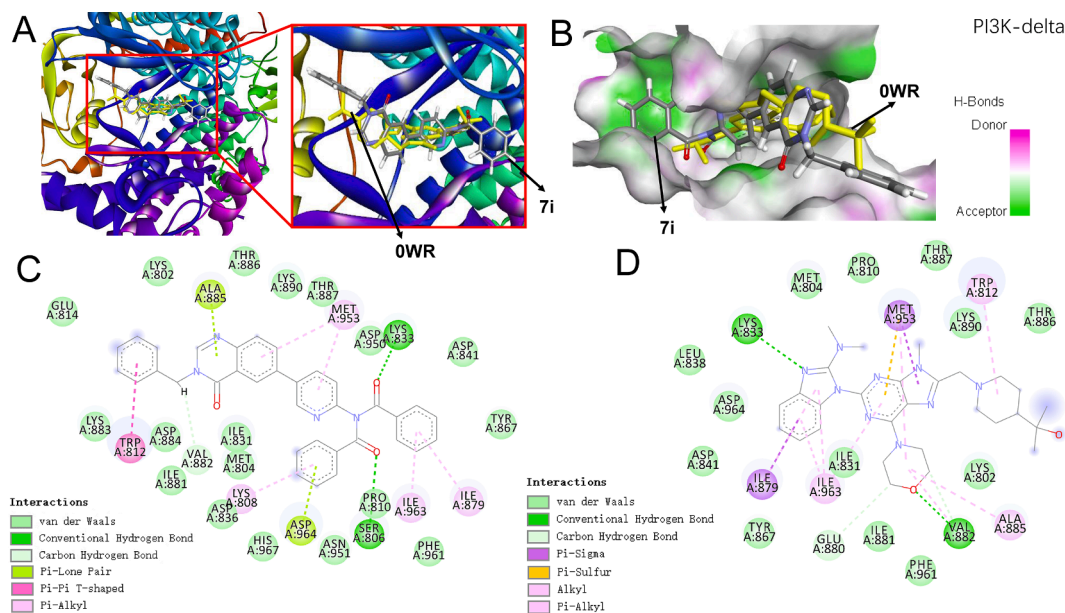
3.1.1. Experimental general information

All reagents and solvents were commercially available and were used without further purification. ^1H NMR and ^{13}C NMR spectra were recorded on a Bruker AVANCE NEO 600 MHz NMR spectrometer and the NMR spectra was generated using Mestrenova 12.0 as processing software. Spectra were recorded at 25 °C using dimethyl sulfoxide- d_6 and chloroform- d as solvents with tetramethylsilane (TMS) as an internal standard. All chemical shifts are reported in ppm (d), and coupling constants (J) are in hertz (Hz). All the melting points were determined

on a Beijing micro meltingpoint apparatus, and the values are uncorrected. High-resolution exact mass measurements were performed using electrospray ionization (positive mode) on a quadrupole time-of-flight (QTOF) mass spectrometer (micro TOF-Q, Bruker Inc.). The structures of compounds **7a** to **7o** were confirmed based on ^1H and ^{13}C NMR spectroscopy, HR-MS and element analysis.

3.1.2. General procedure for the preparation of **7a-7o**

3.1.2.1. Preparation of 6-bromo- N^3 -substituted quinazolin-4(3H)-ones, method A. A mixture of 2-amino-5-bromobenzoic acid (2.16 g, 10 mmol) and formamide (1.80 g, 40 mmol) was heated at 130 °C. After the mixture had been stirred for 4 h, water (30 mL) was added. The reaction



mixture was cooled to 60 °C, and additional water (20 mL) was added to the mixture. After stirring the mixture for another 30 min, the precipitated product was separated by vacuum filtration. The crude products were recrystallized from ethanol to give *6-bromoquinazolin-4(3H)-one 2* as a white solid (1.97 g, 8.76 mmol, 87.6% yield). ESI-MS: m/z 224.3, 226.3 $[M + H]^+$. To a solution of compound **2** (1.13 g, 5 mmol) in anhydrous DMF 15 mL under argon was added NaH (60% dispersion in

mineral oil, 0.24 g, 6 mmol) in one portion. The reaction mixture was stirred at room temperature for 3 min, and then 2-chloro-1-morpholinoethan-1-one (1.15 g, 7 mmol) was added dropwise. The reaction mixture was stirred at room temperature overnight and then partitioned between EtOAc (100 mL) and brine (100 mL). The organic layer was washed with more brine (100 mL). The combined aqueous washings were extracted with EtOAc (3 \times 75 mL). The combined AcOEt extracts

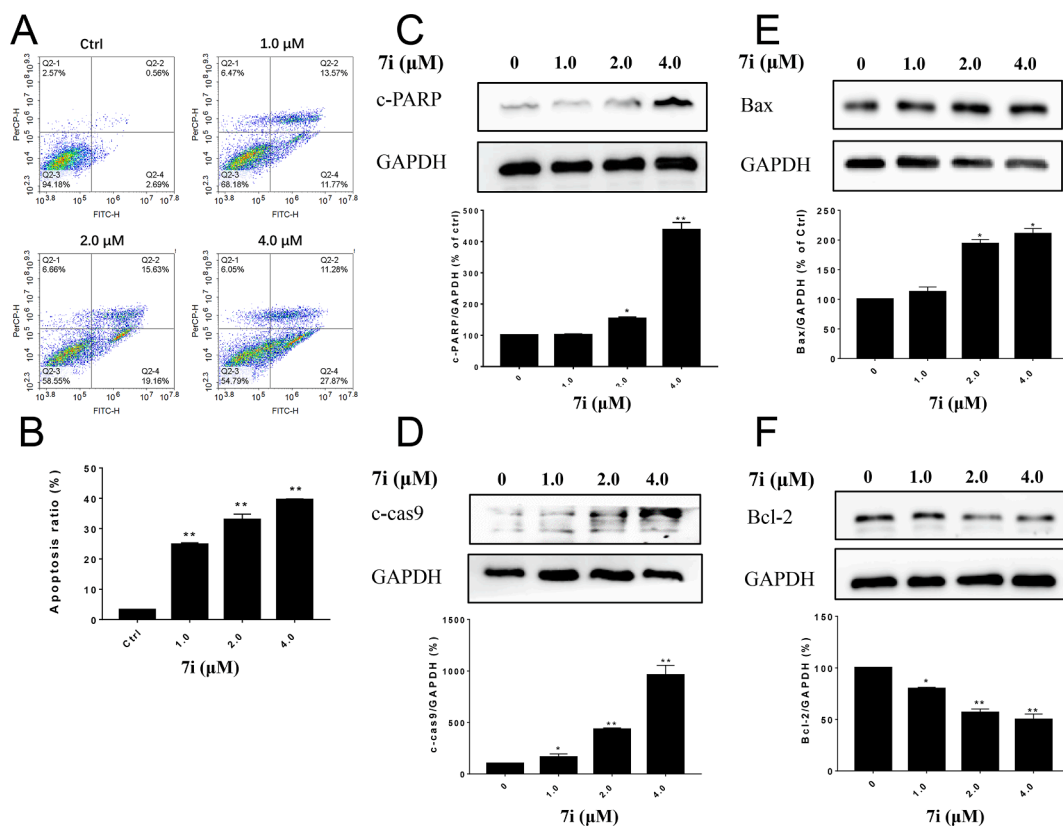


Figure 8. The effects of compound **7i** on cell apoptosis. (A–B) Compound **7i** induced apoptosis in HCC827 cells. Cells were treated with various concentrations of **7i** for 48 h and then analyzed the Annexin V-FITC/PI staining test by flow cytometry analysis. The number in the right quadrants of each panel means the percentage of Annexin V positive cells. (C–F) Representative protein expression in compound **7i** treated cells to investigate the effects of **7i** on the alteration of mitochondrial apoptosis. GAPDH was employed as the loading control. The changes of corresponding proteins were quantified using Image J. Each bar represents mean \pm SD ($n = 3$), * $P < 0.05$ or ** $P < 0.01$ was considered statistically significant compared with corresponding control values.

were washed with brine (2×100 mL), dried (MgSO_4), and concentrated in vacuo. Purification by column chromatography eluting with EtOAc/PE, afforded **6-bromo-3-(2-morpholino-2-oxoethyl) quinazolin-4(3H)-one 4a** as a white solid (1.21 g, 3.44 mmol, 68.8% yield). ESI-MS: m/z 352.0, 354.0 $[\text{M} + \text{H}]^+$.

3.1.2.2. Preparation of 6-bromo- N^3 -substituted quinazolin-4(3H)-ones, method B. The mixture of 2-amino-5-bromobenzoic acid (2.16 g, 10 mmol), triethyl orthoformate (1.93 g, 13 mmol), benzo[d][1,3]dioxol-5-ylmethanamine (1.97 g, 13 mmol), iodine (0.025 g, 0.1 mmol) and anhydrous ethanol (30 mL) was refluxed under argon atmosphere for 4–6 h, then concentrated under vacuum to give a residue which was dissolved in ethyl acetate (100 mL). The ethyl acetate solution was washed with 1 N aqueous sodium hydroxide (50 mL \times 3) and brine (50 mL \times 3), dried over anhydrous sodium sulfate and concentrated to give **3-(benzo[d][1,3]dioxol-5-ylmethyl)-6-bromoquinazolin-4(3H)-one 4b** as white solid (2.809 g, 7.82 mmol, 78.2% yield). ESI-MS: m/z 382.0, 384.0 $[\text{M} + \text{Na}]^+$.

Compounds **4c–4f** were synthesized according to the procedure described in **4b**. The ESI-MS information of compounds **4c–4f** was listed as below:

3-benzyl-6-bromoquinazolin-4(3H)-one (4c)

White solid, 86.0% yield. ESI-MS m/z : 338.0, 340.0 $[\text{M} + \text{Na}]^+$.

6-bromo-3-(4-methylbenzyl) quinazolin-4(3H)-one (4d)

White solid, 88.0% yield. ESI-MS: m/z 352.0, 354.0 $[\text{M} + \text{H}]^+$.

6-bromo-3-butylquinazolin-4(3H)-one (4e)

White solid, 81.1% yield. ESI-MS: m/z 281.0, 283.0 $[\text{M} + \text{H}]^+$.

6-bromo-3-(2-morpholinoethyl) quinazolin-4(3H)-one (4f)

White solid, 72.1% yield. ESI-MS: m/z 338.0, 340.0 $[\text{M} + \text{H}]^+$.

3.1.2.3. 6-(6-aminopyridin-3-yl)-3-(2-morpholino-2-oxoethyl) quinazolin-4(3H)-one (6a). A solution of 5-(4,4,5,5-tetramethyl-1,3,2-dioxaborolan-2-yl) pyridin-2-amine **5** (1.10 g, 5 mmol), 6-bromoquinazolin-4(3H)-one **4a** (1.76 g, 5 mmol), and K_2CO_3 (2.07 g, 15 mmol), 1,4-dioxane/water 25 mL $[\text{V}(\text{dioxane}) : \text{V}(\text{water}) = 4 : 1]$ mixture as solvent was heated to 100 °C and stirred for 15 min. $\text{Pd}(\text{dppf})\text{Cl}_2$ (0.18 g, 0.25 mmol) was added, and the mixture was continued stirred at this temperature under argon for another 4–6 h. 1,4-dioxane and water was removed under reduced pressure and the residue was purified through a column chromatography on silica with dichloromethane/methanol to give **6-(6-aminopyridin-3-yl)-3-(2-morpholino-2-oxoethyl) quinazolin-4(3H)-one 6a** as gray solid (1.611 g, 4.41 mmol, 88.1% yield). ESI-MS: m/z 366.0 $[\text{M} + \text{H}]^+$.

Compounds **6b–6f** were synthesized according to the procedure described in **6a**. The ESI-MS information of compounds **6b–6f** was listed as below:

6-(6-aminopyridin-3-yl)-3-(benzo[d][1,3]dioxol-5-ylmethyl) quinazolin-4(3H)-one (6b)

White solid, 83.2% yield. ESI-MS: m/z 395.1 $[\text{M} + \text{Na}]^+$.

6-(6-aminopyridin-3-yl)-3-benzylquinazolin-4(3H)-one (6c)

White solid, 86.0% yield. ESI-MS: m/z 329.0 $[\text{M} + \text{H}]^+$.

6-(6-aminopyridin-3-yl)-3-(4-methylbenzyl) quinazolin-4(3H)-one (6d)

White solid, 88.7% yield. ESI-MS: m/z 365.1 $[\text{M} + \text{Na}]^+$.

6-(6-aminopyridin-3-yl)-3-butylquinazolin-4(3H)-one (6e)

White solid, 88.0% yield. ESI-MS: m/z 295.1 $[\text{M} + \text{H}]^+$.

6-(6-aminopyridin-3-yl)-3-(2-morpholinoethyl) quinazolin-4(3H)-one (6f)

White solid, 88.4% yield. ESI-MS: m/z 352.1 $[\text{M} + \text{H}]^+$.

3.1.2.4. *N*-(5-(3-(2-morpholino-2-oxoethyl)-4-oxo-3,4-dihydroquinazolin-6-yl) pyridin-2-yl) pro-pionamide (7a). A solution of **6a** (0.365 g, 1 mmol) and triethylamine (0.202 g, 2 mmol) in anhydrous tetrahydrofuran (THF, 20 mL) was stirred for 45 min. Subsequently, a solution of propionyl chloride (0.139 g, 1.5 mmol) in THF (5 mL) was added drop wisely to the reaction mixture under ice cold conditions using a dropping funnel and the contents were stirred further for 2 h at ambient temperature. Completion of the reaction was monitored by TLC. The slurry was pulled into saturated salt water 50 mL and extracted with dichloromethane (50 mL × 3), the combined organic fractions were washed with saturated NaHCO₃ aqueous solution three times, dried over MgSO₄ and the solvent was removed under reduced pressure to obtain a solid residue which was purified through a column chromatography on silica with dichloromethane/methanol to afford **7a**, as a white solid (0.229 g, 0.543 mmol, 54.3% yield), mp 189–191 °C, ¹H NMR (600 MHz, DMSO-*d*₆) δ 10.60 (s, 1H), 8.74 (s, 1H), 8.37 (d, *J* = 6.6 Hz, 1H), 8.27 (s, 1H), 8.21 (d, *J* = 3.9 Hz, 2H), 8.20 (s, 1H), 7.79 (d, *J* = 8.4 Hz, 1H), 4.98 (s, 2H), 3.69 (s, 2H), 3.60 (s, 4H), 3.47 (s, 2H), 2.43 (q, *J* = 7.5 Hz, 2H), 1.09 (t, *J* = 7.5 Hz, 3H). ¹³C NMR (151 MHz, DMSO-*d*₆) δ 173.1, 165.2, 160.1, 151.9, 148.7, 147.4, 146.0, 136.4, 132.6, 129.6, 128.1, 123.0, 121.9, 113.3, 66.0, 46.6, 45.6, 44.8, 42.1, 40.1, 29.4, 9.4. HRMS (ESI): C₂₂H₂₄O₄N₅ [M + H]⁺ *m/z*: calcd. for 422.1823, found 422.1813.

Compounds **7b–7o** were synthesized according to the procedure described in **7a**.

3.1.2.5. *N*-(5-(3-(benzo[*d*] [1,3] dioxol-5-ylmethyl)-4-oxo-3,4-dihydroquinazolin-6-yl) pyridin-2-yl) propionamide (7b). White solid, 53.2% yield, mp 172–174 °C, ¹H NMR (600 MHz, DMSO-*d*₆) δ 10.60 (s, 1H), 8.74 (s, 1H), 8.59 (s, 1H), 8.39 (s, 1H), 8.21 (s, 2H), 8.18 (d, *J* = 8.5 Hz, 1H), 7.77 (d, *J* = 8.5 Hz, 1H), 7.04 (s, 1H), 6.92 (d, *J* = 8.1 Hz, 1H), 6.88 (d, *J* = 8.0 Hz, 1H), 5.99 (s, 2H), 5.12 (s, 2H), 2.43 (q, *J* = 7.6 Hz, 2H), 1.08 (t, *J* = 7.6 Hz, 3H). ¹³C NMR (151 MHz, DMSO-*d*₆) δ 173.1, 160.1, 151.9, 148.0, 147.4, 147.2, 146.9, 146.0, 136.4, 135.6, 132.5, 130.5, 129.5, 128.1, 123.1, 122.1, 121.7, 113.2, 108.7, 108.3, 101.1, 48.8, 29.4, 9.4. HRMS (ESI): C₂₄H₂₁O₄N₄ [M + H]⁺ *m/z*: calcd. for 429.1557, found 429.1549.

3.1.2.6. *N*-(5-(3-(benzo[*d*] [1,3] dioxol-5-ylmethyl)-4-oxo-3,4-dihydroquinazolin-6-yl) pyridin-2-yl) pentanamide (7c). White solid, 54.1% yield, mp 191–193 °C, ¹H NMR (600 MHz, DMSO-*d*₆) δ 10.61 (s, 1H), 8.73 (s, 1H), 8.59 (s, 1H), 8.36 (d, *J* = 8.7 Hz, 1H), 8.21 (d, *J* = 9.1 Hz, 1H), 8.20–8.19 (m, 1H), 8.18 (d, *J* = 8.4 Hz, 1H), 7.77 (d, *J* = 8.5 Hz, 1H), 7.04 (s, 1H), 6.92 (d, *J* = 8.0 Hz, 1H), 6.88 (d, *J* = 8.0 Hz, 1H), 5.98 (s, 2H), 5.12 (s, 2H), 2.42 (t, *J* = 7.4 Hz, 2H), 1.61–1.54 (m, 2H), 1.32 (dq, *J* = 14.6, 7.3 Hz, 2H), 0.89 (t, *J* = 7.3 Hz, 3H). ¹³C NMR (151 MHz, DMSO-*d*₆) δ 172.4, 160.1, 151.8, 148.0, 147.4, 146.9, 146.0, 136.4, 135.6, 132.5, 130.5, 128.1, 123.1, 122.1, 121.7, 113.3, 108.7, 108.3, 101.1, 48.7, 45.4, 35.8, 27.1, 21.8, 13.7, 8.5. HRMS (ESI): C₂₆H₂₅O₄N₄ [M + H]⁺ *m/z*: calcd. for 457.1870, found 457.1854.

3.1.2.7. *N*-(5-(3-(benzo[*d*] [1,3] dioxol-5-ylmethyl)-4-oxo-3,4-dihydroquinazolin-6-yl) pyridin-2-yl) pivalamide (7d). White solid, 54.5% yield, mp 193–195 °C, ¹H NMR (600 MHz, DMSO-*d*₆) δ 9.95 (s, 1H), 8.74 (s, 1H), 8.58 (s, 1H), 8.39 (d, *J* = 2.0 Hz, 1H), 8.18 (s, 2H), 8.16 (dd, *J* = 8.5, 2.0 Hz, 1H), 7.76 (d, *J* = 8.5 Hz, 1H), 7.03 (d, *J* = 1.1 Hz, 1H), 6.92 (dd, *J* = 8.0, 1.1 Hz, 1H), 6.87 (d, *J* = 8.0 Hz, 1H), 5.98 (s, 2H), 5.11 (s, 2H), 1.25 (s, 9H, 3 × CH₃). ¹³C NMR (151 MHz, DMSO-*d*₆) δ 179.4, 177.3, 160.1, 152.0, 148.1, 147.3, 145.7, 136.8, 136.2, 135.6, 132.5, 129.7, 128.6, 128.1, 127.7, 123.1, 122.1, 121.7, 114.0, 108.7, 108.3, 101.1, 49.0, 37.7, 22.1, 13.9. HRMS (ESI): C₂₆H₂₅O₄N₄ [M + H]⁺ *m/z*: calcd. for 457.1870, found 457.1863.

3.1.2.8. *N*-(5-(3-benzyl-4-oxo-3,4-dihydroquinazolin-6-yl) pyridin-2-yl) pentanamide (7e). White solid, 55.2% yield, mp 197–199 °C, ¹H NMR (600 MHz, DMSO-*d*₆) δ 10.61 (s, 1H), 8.73 (s, 1H), 8.62 (s, 1H), 8.38 (d,

J = 2.1 Hz, 1H), 8.21–8.19 (m, 2H), 8.17 (d, *J* = 2.1 Hz, 1H), 7.78 (d, *J* = 8.5 Hz, 1H), 7.38 (d, *J* = 7.3 Hz, 2H), 7.35 (t, *J* = 7.6 Hz, 2H), 7.28 (t, *J* = 7.2 Hz, 1H), 5.23 (s, 2H), 2.41 (t, *J* = 7.4 Hz, 2H), 1.59–1.55 (m, 2H), 1.32 (d, *J* = 7.5 Hz, 1H), 1.30 (d, *J* = 7.4 Hz, 1H), 0.89 (t, *J* = 7.4 Hz, 3H). ¹³C NMR (151 MHz, DMSO-*d*₆) δ 172.4, 160.1, 151.8, 148.2, 147.3, 146.0, 136.8, 136.4, 135.7, 132.5, 129.6, 128.7, 128.2, 127.7, 123.1, 122.1, 113.3, 49.0, 35.8, 27.1, 25.1, 21.8, 13.8. HRMS (ESI): C₂₅H₂₅O₂N₄ [M + H]⁺ *m/z*: calcd. for 413.1972, found 413.1960.

3.1.2.9. *N*-(5-(3-benzyl-4-oxo-3,4-dihydroquinazolin-6-yl) pyridin-2-yl) pivalamide (7f). White solid, 55.8% yield, mp 144–146 °C, ¹H NMR (600 MHz, DMSO-*d*₆) δ 9.97 (s, 1H), 8.75 (d, *J* = 2.0 Hz, 1H), 8.61 (s, 1H), 8.40 (d, *J* = 1.7 Hz, 1H), 8.19 (d, *J* = 5.3 Hz, 2H), 8.17 (s, 1H), 7.79 (d, *J* = 8.5 Hz, 1H), 7.38 (d, *J* = 7.3 Hz, 2H), 7.35 (t, *J* = 7.5 Hz, 2H), 7.29 (t, *J* = 7.1 Hz, 1H), 5.23 (s, 2H), 1.26 (s, 9H, 3 × CH₃). ¹³C NMR (151 MHz, DMSO-*d*₆) δ 177.3, 160.1, 152.0, 148.2, 147.3, 145.7, 136.8, 136.3, 135.6, 132.6, 129.7, 128.7, 128.2, 127.7, 123.1, 122.1, 121.7, 114.0, 108.7, 108.3, 101.1, 49.0, 40.1, 26.9, 25.0. HRMS (ESI): C₂₅H₂₅O₂N₄ [M + H]⁺ *m/z*: calcd. for 413.1972, found 413.1960.

3.1.2.10. *N*-(5-(3-benzyl-4-oxo-3,4-dihydroquinazolin-6-yl) pyridin-2-yl) propionamide (7g). White solid, 54.7% yield, mp 156–158 °C, ¹H NMR (600 MHz, DMSO-*d*₆) δ 10.60 (s, 1H), 8.74 (t, *J* = 1.6 Hz, 1H), 8.61 (s, 1H), 8.40 (d, *J* = 2.2 Hz, 1H), 8.21 (t, *J* = 2.0 Hz, 3H), 7.79 (d, *J* = 8.5 Hz, 1H), 7.37 (dt, *J* = 15.1, 7.4 Hz, 6H), 5.23 (s, 2H), 1.08 (t, *J* = 7.5 Hz, 4H). ¹³C NMR (151 MHz, DMSO-*d*₆) δ 173.1, 160.1, 151.9, 148.1, 147.4, 147.3, 146.0, 136.9, 136.8, 136.4, 135.7, 132.6, 129.5, 128.7, 128.2, 127.7, 123.1, 122.1, 113.2, 49.0, 40.1, 29.4, 9.4. HRMS (ESI): C₂₃H₂₁O₂N₄ [M + H]⁺ *m/z*: calcd. for 385.1659, found 385.1649.

3.1.2.11. *N*-(5-(3-benzyl-4-oxo-3,4-dihydroquinazolin-6-yl) pyridin-2-yl)-2-methoxyacetamide (7h). White solid, 53.8% yield, mp 147–149 °C, ¹H NMR (600 MHz, CDCl₃) δ 10.18 (s, 1H), 8.75 (d, *J* = 2.3 Hz, 1H), 8.61 (s, 1H), 8.39 (d, *J* = 2.1 Hz, 1H), 8.24 (dd, *J* = 8.7, 2.4 Hz, 1H), 8.21–8.17 (m, 2H), 7.79 (d, *J* = 8.5 Hz, 1H), 7.38 (d, *J* = 7.2 Hz, 2H), 7.35 (t, *J* = 7.6 Hz, 2H), 7.29 (t, *J* = 7.1 Hz, 1H), 5.23 (s, 2H), 4.10 (s, 2H), 3.38 (s, 3H). ¹³C NMR (151 MHz, DMSO-*d*₆) δ 168.8, 160.1, 150.9, 148.2, 147.3, 146.1, 136.8, 136.6, 135.5, 132.6, 130.1, 128.7, 128.2, 127.7, 123.3, 122.1, 113.4, 71.2, 58.7, 49.0. HRMS (ESI): C₂₃H₂₁O₃N₄ [M + H]⁺ *m/z*: calcd. for 401.1608, found 401.1600.

3.1.2.12. *N*-benzoyl-*N*-(5-(3-benzyl-4-oxo-3,4-dihydroquinazolin-6-yl) pyridin-2-yl) benzamide (7i). White solid, 56.3% yield, mp 166–168 °C, ¹H NMR (600 MHz, CDCl₃) δ 8.74 (d, *J* = 2.3 Hz, 1H), 8.63 (s, 1H), 8.39 (d, *J* = 2.1 Hz, 1H), 8.36 (dd, *J* = 8.4, 2.5 Hz, 1H), 8.19 (dd, *J* = 8.5, 2.2 Hz, 1H), 7.81 (s, 2H), 7.80 (d, *J* = 1.2 Hz, 2H), 7.78 (d, *J* = 8.5 Hz, 1H), 7.74 (d, *J* = 8.4 Hz, 1H), 7.56 (t, *J* = 7.5 Hz, 2H), 7.47 (s, 1H), 7.46 (s, 2H), 7.44 (s, 1H), 7.38 (d, *J* = 7.2 Hz, 2H), 7.35 (t, *J* = 7.5 Hz, 2H), 7.29 (t, *J* = 7.1 Hz, 1H), 5.22 (s, 2H). ¹³C NMR (151 MHz, DMSO-*d*₆) δ 172.8, 160.0, 152.9, 148.5, 147.8, 146.7, 137.0, 136.7, 134.6, 134.3, 132.9, 132.8, 129.1, 128.8, 128.7, 128.2, 127.7, 124.1, 122.4, 122.1, 49.0. HRMS (ESI): C₃₄H₂₅O₃N₄ [M + H]⁺ *m/z*: calcd. for 537.1921, found 537.1909.

3.1.2.13. *N*-(5-(3-(4-methylbenzyl)-4-oxo-3,4-dihydroquinazolin-6-yl) pyridin-2-yl) pentanamide (7j). White solid, 56.6% yield, mp 213–215 °C, ¹H NMR (600 MHz, DMSO-*d*₆) δ 10.68 (s, 1H), 8.81 (s, 1H), 8.66 (s, 1H), 8.47 (s, 1H), 8.30 (d, *J* = 8.5 Hz, 1H), 8.28 (s, 1H), 8.26 (s, 1H), 7.86 (d, *J* = 8.4 Hz, 1H), 7.36 (d, *J* = 7.6 Hz, 2H), 7.24 (d, *J* = 7.5 Hz, 2H), 5.26 (s, 2H), 2.59 (s, 2H), 2.34 (s, 3H), 1.71–1.62 (m, 2H), 1.42 (d, *J* = 7.3 Hz, 1H), 1.40–1.36 (m, 1H), 0.98 (t, *J* = 7.2 Hz, 3H). ¹³C NMR (151 MHz, DMSO-*d*₆) δ 172.5, 160.1, 151.9, 148.1, 147.3, 146.0, 137.1, 136.4, 135.7, 133.9, 132.6, 129.6, 129.3, 128.2, 127.8, 123.2, 122.2, 113.4, 48.8, 35.9, 27.2, 21.8, 20.7, 13.8. HRMS (ESI): C₂₆H₂₇O₂N₄ [M + H]⁺ *m/z*: calcd. for 427.2129, found 427.2123.

3.1.2.14. *N*-(5-(3-(4-methylbenzyl)-4-oxo-3,4-dihydroquinazolin-6-yl)pyridin-2-yl) propionamide (**7k**). White solid, 55.4% yield, mp 187–189 °C, ¹H NMR (600 MHz, CDCl₃) δ 10.59 (s, 1H), 8.72 (s, 1H), 8.57 (s, 1H), 8.37 (d, *J* = 1.7 Hz, 1H), 8.21 (d, *J* = 8.6 Hz, 1H), 8.19–8.14 (m, 2H), 7.76 (d, *J* = 8.5 Hz, 1H), 7.28 (d, *J* = 8.0 Hz, 2H), 7.15 (d, *J* = 7.8 Hz, 2H), 5.17 (s, 2H), 2.43 (q, *J* = 7.5 Hz, 2H), 2.25 (s, 3H), 1.08 (t, *J* = 7.5 Hz, 3H). ¹³C NMR (151 MHz, DMSO-*d*₆) δ 173.0, 160.0, 151.8, 148.0, 147.2, 145.9, 137.0, 136.3, 135.6, 133.8, 132.5, 129.5, 129.2, 128.1, 127.8, 123.1, 122.1, 113.2, 48.7, 29.4, 20.7, 9.4. HRMS(ESI): C₂₄H₂₃O₂N₄ [M + H]⁺ *m/z*: calcd. for 399.1816, found 399.1807.

3.1.2.15. *N*-benzoyl-*N*-(5-(3-(4-methylbenzyl)-4-oxo-3,4-dihydroquinazolin-6-yl)pyridin-2-yl) ben-zamide (**7l**). White solid, 56.3% yield, mp 166–168 °C, ¹H NMR (600 MHz, DMSO-*d*₆) δ 8.73 (s, 1H), 8.59 (s, 1H), 8.38 (s, 1H), 8.35 (d, *J* = 7.7 Hz, 1H), 8.18 (d, *J* = 8.0 Hz, 1H), 7.80 (d, *J* = 7.2 Hz, 4H), 7.77 (d, *J* = 8.7 Hz, 1H), 7.73 (d, *J* = 8.2 Hz, 1H), 7.55 (d, *J* = 6.9 Hz, 2H), 7.45 (t, *J* = 7.0 Hz, 4H), 7.27 (d, *J* = 7.3 Hz, 2H), 7.15 (d, *J* = 7.1 Hz, 2H), 5.17 (s, 2H), 2.25 (s, 3H). ¹³C NMR (151 MHz, DMSO-*d*₆) δ 172.8, 160.0, 152.9, 148.5, 147.8, 146.7, 137.1, 137.1, 134.7, 134.4, 133.8, 133.0, 132.9, 132.8, 129.2, 129.1, 128.9, 128.3, 127.8, 124.1, 122.5, 122.2, 48.8, 20.7. HRMS(ESI): C₃₅H₂₇O₃N₄ [M + H]⁺ *m/z*: calcd. for 551.2078, found 551.2065.

3.1.2.16. *N*-(5-(3-butyl-4-oxo-3,4-dihydroquinazolin-6-yl)pyridin-2-yl) propionamide (**7m**). White solid, 55.7% yield, mp 123–125 °C, ¹H NMR (600 MHz, DMSO-*d*₆) δ 10.59 (s, 1H), 8.73 (s, 1H), 8.41 (s, 1H), 8.38 (d, *J* = 1.9 Hz, 1H), 8.21 (d, *J* = 8.6 Hz, 1H), 8.19 (dd, *J* = 8.8, 2.2 Hz, 1H), 8.17 (dd, *J* = 8.5, 2.0 Hz, 1H), 7.76 (d, *J* = 8.5 Hz, 1H), 4.00 (t, *J* = 7.2 Hz, 2H), 2.43 (q, *J* = 7.5 Hz, 2H), 1.71–1.67 (m, 2H), 1.33 (d, *J* = 7.5 Hz, 1H), 1.31 (d, *J* = 7.4 Hz, 1H), 1.09 (t, *J* = 7.5 Hz, 3H), 0.91 (t, *J* = 7.4 Hz, 3H). ¹³C NMR (151 MHz, CDCl₃) δ 172.6, 161.2, 151.2, 147.7, 146.9, 146.2, 137.1, 136.6, 132.6, 131.4, 128.5, 124.4, 122.8, 114.0, 47.1, 31.6, 31.0, 20.0, 13.8, 9.5. HRMS(ESI): C₂₀H₂₃O₂N₄ [M + H]⁺ *m/z*: calcd. for 351.1816, found 351.1810.

3.1.2.17. *N*-(5-(3-(2-morpholinoethyl)-4-oxo-3,4-dihydroquinazolin-6-yl)pyridin-2-yl) propionamide (**7n**). White solid, 56.3% yield, mp 110–112 °C, ¹H NMR (600 MHz, DMSO-*d*₆) δ 10.58 (s, 1H), 8.73 (d, *J* = 2.1 Hz, 1H), 8.38 (d, *J* = 2.2 Hz, 1H), 8.34 (s, 1H), 8.21 (s, 1H), 8.19 (dd, *J* = 8.8, 2.4 Hz, 1H), 8.17 (dd, *J* = 8.5, 2.2 Hz, 1H), 7.76 (d, *J* = 8.5 Hz, 1H), 4.11 (t, *J* = 6.0 Hz, 2H), 3.54–3.51 (m, 4H), 2.62 (t, *J* = 6.0 Hz, 2H), 2.44 (d, *J* = 3.3 Hz, 2H), 2.43 (s, 2H), 2.41 (d, *J* = 7.6 Hz, 2H), 1.09 (t, *J* = 7.5 Hz, 3H). ¹³C NMR (151 MHz, DMSO-*d*₆) δ 173.1, 151.8, 147.3, 145.9, 136.4, 132.4, 129.6, 128.1, 123.0, 122.0, 113.3, 53.2, 45.3, 29.4, 9.4, 8.4. HRMS(ESI): C₂₂H₂₆O₃N₅ [M + H]⁺ *m/z*: calcd. for 408.2030, found 408.2025.

3.1.2.18. *N*-(5-(3-(2-morpholinoethyl)-4-oxo-3,4-dihydroquinazolin-6-yl)pyridin-2-yl) pentanamide (**7o**). White solid, 56.7% yield, mp 162–164 °C, ¹H NMR (600 MHz, DMSO-*d*₆) δ 10.60 (s, 1H), 8.73 (d, *J* = 1.5 Hz, 1H), 8.38 (d, *J* = 2.0 Hz, 1H), 8.35 (s, 1H), 8.22 (d, *J* = 8.7 Hz, 1H), 8.20–8.19 (m, 1H), 8.17 (dd, *J* = 8.6, 2.2 Hz, 1H), 7.76 (d, *J* = 8.5 Hz, 1H), 4.11 (t, *J* = 6.0 Hz, 2H), 3.54–3.51 (m, 4H), 2.62 (t, *J* = 6.0 Hz, 2H), 2.43 (d, *J* = 6.6 Hz, 4H), 2.41 (d, *J* = 7.5 Hz, 2H), 1.60–1.56 (m, 2H), 1.33 (d, *J* = 7.5 Hz, 1H), 1.31 (d, *J* = 7.4 Hz, 1H), 0.89 (t, *J* = 7.4 Hz, 3H). ¹³C NMR (151 MHz, DMSO-*d*₆) δ 172.4, 160.1, 151.8, 148.5, 147.3, 146.0, 136.4, 135.4, 132.4, 129.6, 128.0, 123.0, 122.0, 113.3, 66.3, 56.3, 53.2, 42.7, 40.1, 35.8, 27.1, 25.1, 21.8, 13.8. HRMS(ESI): C₂₄H₃₀O₃N₅ [M + H]⁺ *m/z*: calcd. for 436.2343, found 436.2334.

3.2. Molecular modeling

To predict the binding mode of **7i** and four subtypes of PI3K, MOE (Molecular Operating Environment) and crystal structures of PI3Kα (PDB entry code: 4ZOP), PI3Kβ (PDB entry code: 4BFR), PI3Kγ (PDB

entry code: 4ANW) and PI3Kδ (PDB entry code: 4GB9) in complex with their ligands were used for molecular modeling. The protein optimizations were carried out using quickprep of MOE and the optimizations of the geometry of the ligands and compound **7i** were performed using the field strengths in the MMFF94x implanted software MOE. The active site was generated by using the site finder option of MOE (Molecular Operating Environment) software based on the co-crystalline ligands. Accelrys Discovery Studio Visualizer 4.5 was used for graphic display.

3.3. Anticancer assay

3.3.1. Cell lines and culture medium

The human non-small cell lung cancer (NSCLC) HCC827, human red and white cell leukemia cell HEL, human neuroblastoma SH-SY5Y and human normal liver HL-7702 cells were obtained from Cell Bank of the Chinese Academy of Sciences (Shanghai, China). The hepatocellular carcinoma LM3 cells were a kind gift of professor Qingchun Zhao. HCC827, HEL, SH-SY5Y and HL-7702 cells were cultured in Roswell Park Memorial Institute (RPMI, Gibco) 1640 medium with 10% fetal bovine serum (FBS, BI) and antibiotics-antimycotics (100 units/mL penicillin G sodium, 100 µg/mL streptomycin, and 250 ng/mL amphotericin B). LM3 cells were cultured in dulbecco's modified eagle medium (DMEM, Gibco) containing 10% FBS and antibiotics-antimycotics. Cells were incubated with 5% CO₂ in a humidified atmosphere at 37 °C.

3.3.2. Cell viability assay

Cell viability assay was performed using cell counting by flow cytometry. Succinctly put, cells of 2.5–3 × 10⁴/well cells were cultured adherently with fresh medium in 12-well plates for 24 h before exposure to various concentrations of compound **7a** to **7o** for 72 h. Then, the cell numbers of living cells were measured by flow cytometry. Data were analyzed using the SPSS, which calculated the half maximal inhibitory concentration (IC₅₀) for each drug.

3.4. Flow cytometry analysis

Cells cycle analysis and Annexin FITC/PI assay were performed as described previously.^{22,23} Briefly, cells were cultured with fresh medium without FBS for 12 h before treatment with compound **7i** for 24 h. The treated cells were fixed with 70% ethanol overnight before staining with propidium iodide mixed with RNase. Keep the dying cells under dark conditions at room temperature for 30 min before being subjected to flow cytometry analysis. Cell apoptosis was evaluated using Annexin V FITC/PI apoptosis detection kit (BD Biosciences, CA, USA) according to the manufacturer's instruction. The stained cells were incubated for 15 min at room temperature in the dark before analyzing with flow cytometry.

3.5. PI3 kinase inhibition assays

The PI3 kinase assay was measured by Cell PI3 Kinase Activity Photometric Assay Kit (Shanghai Yiji Industrial Co., Ltd, China) following the manufacturer's protocols. In brief, cells were treated with various concentration of compound **7i** for 24 h. The treated cells were washed with Reagent A. Regent B was used to lyse the cells and collected the proteins. Protein concentration was measured by Bradford reagent (Bio-Rad, Hercules, Calif). 100 µg cell lysate protein for each group were used to analyze the kinase activity.

3.6. Western blot

Cells were treated with various concentrations of compound **7i**. Western blot analysis was performed as described previously.^{22–25,39} Blots were imaged by ChemiDoc TM MP Imaging System (Bio-Rad, USA).

4. Conclusions

A series of novel 6-(pyridin-3-yl) quinazolin-4(3H)-one derivatives were designed and synthesized as potential anticancer agents as inhibitors of PI3K/Akt pathway. Among them, compound **7i** showed the most antiproliferative activity against all the tested cells and inhibited the PI3K kinase activity with an IC₅₀ values of 0.072 μM. Furthermore, **7i** induced cell cycle arrest in G2/M phase and cell apoptosis in HCC827 cells. Collectively, the results suggested that **7i** might be a hit compound as inhibitor of PI3K/Akt pathway.

Declaration of Competing Interest

The authors declare that they have no known competing financial interests or personal relationships that could have appeared to influence the work reported in this paper.

Acknowledgments

Financial supported by the Natural Science Foundation of China, grant number Grants 21907020, the Natural Science Foundation of Guizhou Province, grant number QKH [2019]1215, Thousands of Innovative Talents of Guizhou Province (Grant No. GZQ202006081) and the project of Service Enterprise Action Plan of Guizhou Province (Grant No. QKHFQ [2020]4013).

Appendix A. Supplementary material

Supplementary data to this article can be found online at <https://doi.org/10.1016/j.bmc.2021.116346>.

References

- Mahato A, Shanthy N. *Inventi Impact Med Chem.* 2011;2011:1–6.
- Jang CS, Fu FY, Huang KC, Wang CY. *Nature.* 2012;161:400–401.
- Castañer J, Sweetman AJ. *Drugs Future.* 1982;7, 539–539.
- Gelbrich T, Haddow MF, Griesser UJ. *Acta Crystallograph.* 2011;67, 1343–1343.
- Huo S, Yu H, Li C, et al. *Int J Clin Exp Pathol.* 2015;8:15863–15870.
- Pines M. *World J Gastroenterol.* 2014;20:14778–14786.
- Cook JA, Choudhuri R, Degraff W, et al. *Cancer Lett.* 2010;289:119–126.
- Kater AP, Tonino SH, Spiering M, et al. *Blood Cancer J.* 2018;8:16.
- Yue D, Sun X. *Cell Death Dis.* 2018;9:935.
- Huen A, Haverkos BM, Zain J, et al. *Cancers (Basel).* 2020;12:2293.
- Thorpe LM, Yuzugullu H, Zhao JJ. *Nat Rev Cancer.* 2015;15:7–24.
- Yang J, Nie J, Ma X, et al. *Mol Cancer.* 2019;18:26.
- Fruman DA, Chiu H, Hopkins BD, et al. *Cell.* 2017;170:605–635.
- Chen L, Yang L, Yao L, et al. *Nat Commun.* 2018;9:1357.
- Martínez-Sáez O, Chic N, Pascual T, et al. *Breast Cancer Res.* 2020;22:45.
- Alqahtani A, Ayesh HSK, Halawani H. *Cancers (Basel).* 2019;12:93.
- Wang L, Hu H, Pan Y, et al. *PLoS ONE.* 2014;9:88291.
- Hanker AB, Kaklamani V, Arteaga CL. *Cancer Discov.* 2019;9:482–491.
- Mishra R, Patel H, Alanazi S, et al. *Int J Mol Sci.* 2021;22:3464.
- Zhao HF, Wang J, Shao W, et al. *Mol Cancer.* 2017;16:100.
- Fan Y, Ding H, Kim D, et al. *Cancers (Basel).* 2019;11:627.
- Fan YH, Ding HW, Liu DD, et al. *Bioorg Med Chem.* 2018;26:1675–1685.
- Fan YH, Li W, Liu DD, et al. *Eur J Med Chem.* 2017;139:95–106.
- Fan YH, Ding HW, Kim D, et al. *Pharmacol Res.* 2020;160, 105147.
- Fan CC, Zhong T, Yang HR, et al. *Eur J Med Chem.* 2020;190, 112108.
- Marzaro G, Castagliuolo I, Schirato G, et al. *Eur J Med Chem.* 2016;115:416–425.
- Ma CC, Zhang CM, Tang LQ, Liu ZP. *Eur J Med Chem.* 2018;151:9–17.
- Roskoski R. *Pharmacol Res.* 2021;168, 105579.
- Kater AP, Tonino SH, Spiering M, et al. *Blood Cancer J.* 2018;16.
- Takeuchi CS, Kim BG, Blazey CM, et al. *J Med Chem.* 201; 6: 2218–2234.
- Bavetsias V, Skelton LA, Yafai F, et al. *J Med Chem.* 2002;45:3692–3702.
- Chen Y, Tsai HW, Tsai YH, Tseng SH. *J Pediatr Surg.* 2020.
- Zhou Q, Lui VW, Yeo W. *Future Oncol.* 2011;7:1149–1167.
- Jin RY, Tang T, Zhou S, et al. *Bioorg Chem.* 2020;98, 103737.
- Furet P, Guagnano V, Fairhurst RA, et al. *Bioorg Med Chem Lett.* 2013;23:3741–3748.
- Heffron TP, Heald RA, Ndubaku C, et al. *J Med Chem.* 2016;59:985–1002.
- Certal V, Carry JC, Halley F, et al. *J Med Chem.* 2014;57:903–920.
- Chandrasekhar J, Dick R, Van Veldhuizen J, et al. *J Med Chem.* 2018;61:6858–6868.
- Lodola A, Bertolini S, Biagetti M, et al. *J Med Chem.* 2017;60:4304–4315.